Nonintrusive Diagnosis of a PEMFC

Melika Hinaje[1], Olivier Bethoux[2], Guillaume Krebs[2], and Bernard Davat[1]

[1]GREEN Laboratory, Université de Lorraine, Vandoeuvre les Nancy Cedex F-54518, France
[2]Laboratoire de Génie Électrique de Paris, Gif-sur-Yvette F-91192, France

Many reasons may cause malfunction of a proton exchange membrane fuel cell (FC) stack. Moreover, a single defect cell can affect the whole stack functioning; therefore, the localization of this cell is crucial as well as identifying the root causes for such malfunctioning. The diagnosis tool has to be nonintrusive and easy to replicate to a new FC system. This paper explores paths to achieve such monitoring based on the use of the magnetic field induced by the FC stack internal currents. Designing and using a 3-D simulation tool allows to establish a cause and effect relationship between FC defects and specific magnetic signatures. This preliminary work enables to determine the required magnetic sensor accuracy, the sensor orientation and location as well as the experimental precautions for relevant measurements.

Index Terms— **3-D partial differential equation modeling, diagnosis, magnetic field, Maxwell–Stefan diffusion, proton exchange membrane fuel cell (FC).**

I. Introduction

USING polymer electrolyte membrane (PEM) fuel cells (FCs) is an attractive way to produce energy without greenhouse gas. A defect in the FC stack, such as drying, flooding, starvation, active layer deterioration, induces a major negative effect on the operation of the overall energy conversion system (FC and its auxiliaries): performance decreases and may cause the FC system to shut down with possible damages to the PEMFC or to one of the auxiliaries. Identification of the defect and understanding the physical processes involved are essential to diagnose accurately the reduced performance causes. The aim of this paper is to compute the magnetic field created by a PEMFC to identify a specific signature in case of malfunctioning cell.

II. PEMFC Modeling

To predict the FC performance, the unknowns, $w_{\mathrm{H2}}, w_{\mathrm{H2O},a}, w_{\mathrm{H2O},c}, w_{\mathrm{O2}}, w_{\mathrm{N2}}, p_a, p_c, \varphi_m, \varphi$, and $\mathbf{v}$ have to be computed by solving the equations of mathematical physics that describe the overall cell. The nomenclature is given in Table I. Computational domain and geometry parameters are given in Fig. 1 and Table II, respectively.

It is assumed as follows.

1) Three species oxygen, nitrogen, and water are present on the cathode side, while hydrogen and water are considered in the anode side.
2) The PEMFC is operating in steady state and its temperature remains constant and homogeneous all over the cell.
3) Flow is considered laminar.
4) There is no condensation in the cell. The single-phase model described here is sufficient for modeling the mass transport in the porous anode and cathode up to moderately high current densities [1], [2].
5) The membrane is gas-tight.
6) The channels are approximated by straight channels.

Manuscript received May 11, 2014; revised August 24, 2014; accepted August 30, 2014. Date of current version April 22, 2015. Corresponding author: M. Hinaje (e-mail: melika.hinaje@univ-lorraine.fr).

Color versions of one or more of the figures in this paper are available online at http://ieeexplore.ieee.org.

Digital Object Identifier 10.1109/TMAG.2014.2355497

A. Mass and Momentum Balances (Coupled)

In the anode and cathode sides, the transport phenomena are similar; only the species differ. In channels, the velocity $\mathbf{v}$ and the pressure of the gas mixtures are described by Navier–Stokes equations, i.e., the conservation of momentum (1) and the conservation of mass known as mass continuity equation (2). As gas diffusion layer (GDL) and catalyst layer (CL) are porous media, the Navier–Stokes equations have to be modified that leads to the so-called Brinkman equations [3] (3).

In the channel, the following system has to be solved:

$$\begin{cases} \nabla\cdot(\rho_{a,c}\mathbf{v}_{a,c}\otimes\mathbf{v}_{a,c}-\mu_{a,c}\nabla\mathbf{v}_{a,c})=\nabla\cdot\left[\mu_{a,c}(\nabla\mathbf{v}_{a,c})^T\right] \\ \qquad\qquad -\nabla\cdot\left(p_{a,c}+\frac{2}{3}\mu_{a,c}\nabla\cdot\mathbf{v}_{a,c}\right)=0 \quad (1) \\ \nabla\cdot(\rho_{a,c}\mathbf{v}_{a,c})=0 \quad (2) \end{cases}$$

While in the GDLs and in the CLs, the below-stated system of equations needs to be solved:

$$\begin{cases} \nabla\cdot\left(\dfrac{\rho_{a,c}}{\varepsilon_{\mathrm{GDL,CL}}}v_{a,c}\otimes v_{a,c}-\dfrac{\mu_{a,c}}{\varepsilon_{\mathrm{GDL,CL}}}\nabla v_{a,c}\right) \\ =\nabla\cdot\left[\dfrac{\mu_{a,c}}{\varepsilon_{\mathrm{GDL,CL}}}(\nabla v_{a,c})^T\right]-\nabla\cdot\left(p_{a,c}+\dfrac{2}{3}\dfrac{\mu_{a,c}}{\varepsilon_{\mathrm{GDL,CL}}}\nabla\cdot v_{a,c}\right) \quad (3) \\ -\dfrac{\mu_{a,c}}{\kappa_{\mathrm{GDL,Cl}}}=0 \\ \nabla\cdot(\rho_{a,c}\mathbf{v}_{a,c})=0 \quad (4) \end{cases}$$

B. Mass and Specifies Balance

The mass and molar fractions obey the Maxwell–Stefan equations, which describe the multispecies diffusion and convection in channels (5) and (6) and electrodes. Pair of species (i, j) interactions are characterized by the binary diffusion coefficient D_{ij} [4]: to account for the electrodes' porosity, the effective diffusion coefficient D_{ij}^{eff} (9) substitutes the D_{ij} coefficient in (8):

$$\nabla\cdot\left[-\rho\cdot w_i\sum_{j=1}^{e}D_{ij}\left(\nabla x_j+(x_j-w_j)\frac{\nabla p_{a,c}}{p_{a,c}}\right)+w_i\rho\mathbf{v_{a,c}}\right]=R_i$$

0018-9464 © 2015 IEEE. Personal use is permitted, but republication/redistribution requires IEEE permission.
See http://www.ieee.org/publications_standards/publications/rights/index.html for more information.

Authorized licensed use limited to: TONGJI UNIVERSITY. Downloaded on March 26,2024 at 08:56:07 UTC from IEEE Xplore. Restrictions apply.

TABLE I
NOMENCLATURE

Symbol	Quantity
A	Magnetic vector potential [Wb. m^{-1}]
B	Magnetic flux density [T]
C_i	Concentration of species i [$mol.m^{-3}$]
D_{ij}^{eff}	Diffusion coeff. of species i in the species j [$m^2.s^{-1}$]
$D^{m}_{H_2O}$	Diffusion coefficient of water[$m^2.s^{-1}$]
EW	Equivalent weight of membrane [$g.mol^{-1}$]
F	Faraday constant, 96485 [$C.mol^{-1}$]
H	Magnetic field [$A.m^{-1}$]
I	Current [A]
J_{cell}	Current density [$A.m^{-2}$]
L_d, L_m	GDLs and membrane thickness respectively [m]
M_i	Molar mass of the species i [$kg.mol^{-1}$]
N_i	Mass flux of species i [$kg.m^{-2}.s^{-1}$]
P_i	Partial pressure of species i [Pa]
P_{sat}	Saturated pressure [Pa]
P_T	Total pressure ($P = \sum P_i$) [Pa]
$P_{a,c}$	Pressure of the gas mixture at anode or cathode side
R	Universal gas constant, 8,314 [$J.mol^{-1}K^{-1}$]
RH	Relative humidity
$T_{\_pile}$	Temperature of the fuel cell [K]
x_i, w_i	Molar and mass fraction of species i respectively
v	Velocity [$m.s^{-1}$]
z	Length [m]
Greek symbols	
α	Transfer coefficient
ε	porosity
φ	Potential [V]
$\mu_{a,c}$	Coefficient of viscosity of the gas mixture [Pa.s]
μ	Permeability magnetic [$H.m^{-1}$]
λ	Water content in the membrane
ρ_{dry}	Dry density of membrane [$g.m^{-1}$]
$\rho_{a,c}$	Density of the mixture [$kg.m^{-3}$]
σ_{H+}	Electric conductivity of the membrane [$S.m^{-1}$]
Subscript	
a	anode
act	activation
c	cathode
CL	Catalyst layer
e	Electrode
GDL	Gas diffusion layer
i	Species (H_2, H_2O, O_2, N_2)
in	Inlet
OCV	Open circuit voltage
out	Outlet
Superscript	
eff	Effective
0	Standard conditions

$$\mathbf{N}_i = \left[-\rho \cdot w_i \sum_{j=1}^{e} D_{ij} \left(\nabla x_j + (x_j - w_j) \frac{\nabla p_{a,c}}{p_{a,c}} \right) + \rho \mathbf{v_{a,c}} w_i \right] \tag{5}$$

(6)

where ρ is the mixture density and D_{ij} is defined by

$$\rho = \left(\sum_{i=1}^{e} x_i M_i \right) \frac{p_{a,c}}{\mathrm{RT}} \tag{7}$$

$$D_{ij} = D_{ij}^{0}(P^0, T^0) \frac{P^0}{T^0} \left(\frac{T}{T^0} \right)^{\frac{3}{2}}. \tag{8}$$

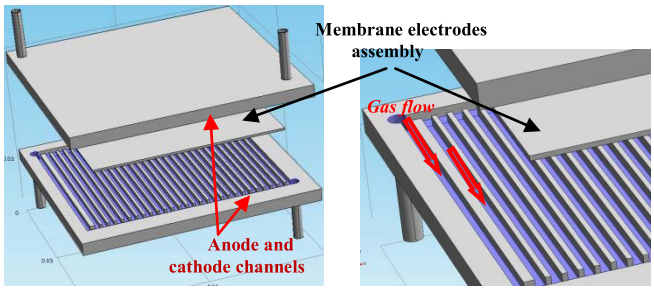

Fig. 1. Single cell element used in the model.

TABLE II
GEOMETRY PARAMETERS

Parameters	Value
Active area	100 cm^2
Anode and cathode GDL thicknesses	380 μm
Membrane thickness	100 μm
Anode and cathode catalyst layer thicknesses	50 μm
GDL porosity	0.4
Catalyst layer porosity	0.3
Anode and cathode channel width	1mm
Cog height of bipolar plates	0.9 mm
GDL conductivity	220 S/m
Membrane conductivity	10 S/m

In the GDLs and CLs, the effective diffusion coefficients are computed by the Bruggeman relation using the Onsager reciprocal relation [5], [6], which leads to

$$D_{ij}^{\mathrm{eff}} = D_{ji}^{\mathrm{eff}} = D_{ij} \varepsilon_{\mathrm{GDL,CL}}^{3/2}. \tag{9}$$

In the continuity (5), species production and consumption are represented by a source term (water production) and a sink term (reactant consumption), respectively. The corresponding R_i term is expressed in kg/($m^3 \cdot$ s). Obviously $R_i = 0$ in flow channels:

$$R_{\mathrm{O_2}} = \frac{j_c}{4F} \mathrm{M_{O_2}} \tag{10}$$

$$R_{\mathrm{H_2}} = -\frac{j_a}{2F} \mathrm{M_{H_2}} \tag{11}$$

$$R_{\mathrm{H_2O}} = -\frac{j_c}{2F} \mathrm{M_{H_2O}} \tag{12}$$

where j_a and j_c are the transfer current densities at CLs.

C. Redox Reaction and Produced Current

Indeed, hydrogen oxidation leads to charges' displacements: a proton one occurs through the membrane inducing an ionic current $j_{\mathrm{H+}}$ while electrons are conducted by the electrodes resulting in an electronic current j_e. Current conservation is expressed as follows:

$$\nabla \cdot j_{\mathrm{cell}} = \nabla \cdot j_e + \nabla \cdot j_{\mathrm{H+}} = 0. \tag{13}$$

Ohm's law links current densities j_i to potentials φ_i:

$$-\sigma_e^{\mathrm{eff}} \nabla \varphi_e = j_{a,c} \tag{14}$$

$$-\sigma_{\mathrm{H+}}^{\mathrm{eff}} \nabla \varphi_{\mathrm{H+}} = j_{a,c}. \tag{15}$$

In (14) and (15), the source terms j_i derive from the electrochemical reactions described by Butler–Volmer equation

$$j_a = a_v j_o^{\mathrm{ref}} \left(\frac{\mathrm{C_{H_2}}}{\mathrm{C_{H_2}^{ref}}} \right)^{1/2} \left[\exp\left(\frac{\alpha_a F}{\mathrm{RT}} \right) \eta_{\mathrm{act}} - \exp\left(-\frac{\alpha_c F}{\mathrm{RT}} \right) \eta_{\mathrm{act}} \right]$$

Authorized licensed use limited to: TONGJI UNIVERSITY. Downloaded on March 26,2024 at 08:56:07 UTC from IEEE Xplore. Restrictions apply.

(16)

$$j_c = a_v j_o^{\text{ref}} \left(\frac{C_{O_2}}{C_{O_2}^{\text{ref}}}\right)\left[\exp\left(\frac{\alpha_a F}{RT}\right)\eta_{\text{act}} - \exp\left(-\frac{\alpha_c F}{RT}\right)\eta_{\text{act}}\right]. \quad (17)$$

The exchange current density j_o^{ref} depends on several parameters such as operating temperature and requires a large number of experiments [7], [8] to be properly identified. η_{act} is the local change of the reversible voltage between electrodes and electrolyte:
At the anode side

$$\eta_{\text{act}} = \varphi_e - \varphi_{\text{H}+}. \quad (18)$$

At the cathode side

$$\eta_{\text{act}} = \varphi_e - \varphi_{\text{H}+} - V_{\text{oc}}. \quad (19)$$

D. Boundary Conditions

The boundary conditions have to be specified for all variables in each domain. In anode and cathode channels, inflows are given by their velocity and their inlet mixtures

$$v_{a,c} = v_{a,c,\text{in}} \quad (20)$$

$$w_a = w_{H_{2,\text{in}}} \quad (21)$$

$$w_c = \begin{cases} w_{O_{2,\text{in}}} \\ w_{H_2O\text{in}}. \end{cases} \quad (22)$$

The outlet boundaries are given by

$$p_{a,c} = p_{\text{out}} \quad (23)$$

and

$$-\mathbf{n}.\left[\rho \cdot w_i \sum_{j=1}^{e} D_{ij}\left(\nabla x_j + (x_j - w_j)\frac{\nabla p_{a,c}}{p_{a,c}}\right)\right] = 0. \quad (24)$$

Elsewhere no slip conditions apply and no flux goes out. Thus

$$-\mathbf{n} \cdot \mathbf{N}_i = 0. \quad (25)$$

The potential is fixed at gas channel-gas diffusion layer interfaces
At the cathode channel interface

$$\varphi_e = V_{\text{cell}}. \quad (26)$$

At the anode channel interface

$$\varphi_e = 0. \quad (27)$$

Initial boundary condition at the membrane

$$\varphi_{\text{H}+} = 0. \quad (28)$$

At the top and at the bottom and on the back and on the front of the FC unique cell, no current goes out. Hence

$$-\mathbf{n} \cdot \mathbf{j_e} = 0 \quad (29)$$

$$-\mathbf{n} \cdot \mathbf{j}_{\text{H}+} = 0. \quad (30)$$

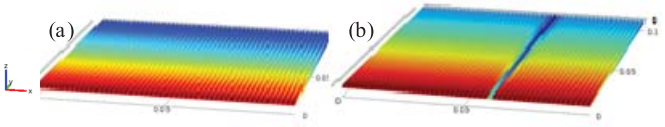

Fig. 2. O_2 diffusion. (a) Healthy cell. (b) Defective cathode channel.

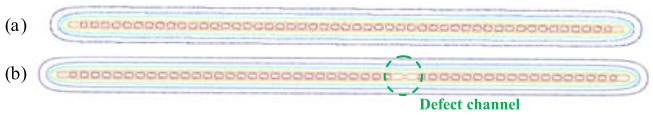

Fig. 3. Magnetic induction tangential component B_x at 0.6 V–31A. xz view of (a) healthy cell and (b) defective cathode channel cell.

E. Magnetic Formulation

As discussed earlier, the main aim of this paper is to propose a set of guiding principles that will support the implementation of nonintrusive FC malfunctioning detection. A default in the heart of the FC might modify the current density repartition and consequently the resulting magnetic field. After computing the FC electrical operating point, the magnetic field is calculated by means of the magnetic vector potential (MVP) (31).

In this part, the studied domain is the single FC Ω_{FC} and the air around it Ω_a. The air domain dimensions are chosen much larger than the cell ones:

$$\Delta \mathbf{A} - \mu_{\mathbf{j}} = \mathbf{0} \quad \text{in } \Omega_a \cup \Omega_{\text{FC}}. \quad (31)$$

To ensure the uniqueness of the solution, a Coulomb gauge (33) has to be coupled to Poisson equation:

$$\nabla \cdot \mathbf{A} = 0. \quad (32)$$

F. Boundary Conditions

The boundary surface is denoted by Γ_{air}. Zero Dirichlet boundary conditions can be applied:

$$\mathbf{A} = \mathbf{0} \text{ on } \Gamma_{\text{air}}. \quad (33)$$

To obtain the PEMFC operating point (V, I), 3-D coupling PDE, describing the mixture gas diffusion and the redox reactions, has to be solved under a given operating condition. Subsequently, the resulting magnetic field is computed by means of MVP. All the equations have been implemented in Comsol software.

III. Some Results

A. Defect Cathode Channel

The considered FC features a 100 cm^2 active area. As one of its cathode channels is blocked, O_2 does no more diffuse correctly (Fig. 2), and consequently, the electrochemical reaction as well as the current distribution are locally disturbed [9]; finally, the resulting magnetic field is modified (Figs. 3 and 4).

B. Defect Anode Channel

The same default is simulated at the anode side; a stopper at the anode channel is located at the top or the middle of the single FC as shown in Fig 5.

Authorized licensed use limited to: TONGJI UNIVERSITY. Downloaded on March 26,2024 at 08:56:07 UTC from IEEE Xplore. Restrictions apply.

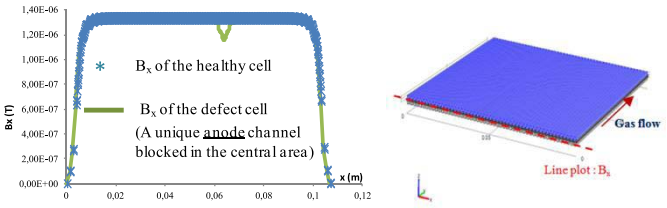

Fig. 4. Comparison between the tangential component of the magnetic induction for a healthy and defective cathode channel.

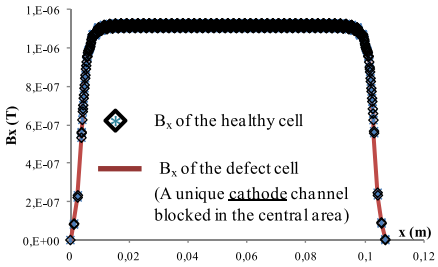

Fig. 5. Comparison between the tangential component of the magnetic induction for a healthy and defective anode channel.

TABLE III
OPERATING CONDITIONS

Parameters	Value
Fuel cell temperature	60 °C
Hydrogen flow rate	624 mL/min
Air flow rate	1.56 L/min
Inlet H_2 mass fraction (anode)	0.743
Inlet O_2 mass fraction (cathode)	0.228
Inlet H_2O mass fraction (cathode)	0.023
Anode inlet flow velocity	0.2 m/s
Cathode inlet flow velocity	0.5 m/s
Anode viscosity	$1.19\ 10^{-5}$ Pa/s
Cathode viscosity	$2.46\ 10^{-5}$ Pa/s
Porous electrode permeability	$1.18\ 10^{-11}$ m²
GDL permeability	$2.36\ 10^{-12}$ m²
H_2-H_2O binary D_{ij}	$1.055\ 10^{-4}$ m²/s
O_2-N_2 binary D_{ij}	$2.751\ 10^{-5}$ m²/s
N_2-H_2O Binary D_{ij}	$2.951\ 10^{-5}$ m/s
O_2-H_2O binary D_{ij}	$3.233\ 10^{-5}$ m/s
Fuel cell voltage	From 0.9 V to 0.6 V

Indeed, due to the stopper, hydrogen diffuses hardly in the default channel. However, for a specified current of 27 A, as shown in Fig. 5, the same default at the anode side does not alter significantly the magnetic field distribution compared with the cathode side.

IV. CONCLUSION

This paper has allowed to build a 3-D computer model of an FC whose originality is to be able to compute the induced magnetic field inside and around the FC. This model has been used in different steady-state scenarios.

Among other things, it permits to compare the magnetic field maps of a good operating cell and a defect one. The final purpose is obviously to determine which defect can be easily detected by magnetic measurement means and to understand the precautions to be taken to achieve relevant measurements and diagnosis.

At a few tens of percent of rated current (a few amps to a few tens of amps for the studied cell), a defect at the cathode can be detected by measuring the tangential component of B with a sensor located closed to the cell. By contrast, a defect placed at the anode side produces a weak effect on the magnetic field B; it would be difficult to achieve a relevant diagnosis of such a situation.

Experimental facility has to be led to demonstrate the scientific and technical feasibility of detecting a cell default among an FC stack. Specifically, the present study shows that, regarding the rated cell current density (approximately $0.5–0.7\ \mathrm{A \cdot cm^{-2}}$), the resulting magnetic field does not exceed the 10^{-6} T range, which can be challenging to measure especially considering that the FC system auxiliaries may distort the measuring results. It is therefore essential to choose a Hall probe featuring a high sensitivity (in the order of milliGauss) with a relatively small active area due to the thickness of a single FC.

According to all these considerations, the experimental setup has to be carried out so that the two current collectors do not disturb the measurement of the magnetic field induced by the FC. One way to do so is to shield magnetically the FC. Another promising way consists in correcting the measurements using the computation of auxiliaries' noises.

In sum, the simulation results allow to check the feasibility of diagnosis by means of magnetic field measurement and size of the test bench and the associated sensors. This experimental stage is a key step and is the next phase of this paper.

ACKNOWLEDGMENT

This work was supported by the Research Group SEEDS.

REFERENCES

[1] M. Hu, A. Gu, M. Wang, X. Zhu, and L. Yu, "Three dimensional, two phase flow mathematical model for PEM fuel cell: Part I. Model development," *Energy Convers. Manage.*, vol. 45, nos. 11–12, pp. 1861–1882, 2004.

[2] M. Hu, A. Gu, M. Wang, X. Zhu, and L. Yu, "Three dimensional, two phase flow mathematical model for PEM fuel cell: Part II. Analysis and discussion of the internal transport mechanisms," *Energy Convers. Manage.*, vol. 45, nos. 11–12, pp. 1883–1916, 2004.

[3] Y.-J. Sohn, M. Kim, T.-H. Yang, and K. Kim, "Numerical analysis of convective and diffusive fuel transports in high-temperature proton-exchange membrane fuel cells," *Int. J. Hydrogen Energy*, vol. 36, no. 23, pp. 15273–15282, 2011.

[4] M. F. Serincan and S. Yesilyurt, "Transient analysis of proton electrolyte membrane fuel cells (PEMFC) at start-up and failure," *Fuel Cells*, vol. 7, no. 2, pp. 118–127, 2007.

[5] M. H. Daneshpajooh, E. A. Mason, E. H. Bresler, and R. P. Wendt, "Equations for membrane transport. Experimental and theoretical tests of the frictional model," *Biophys. J.*, vol. 15, no. 6, pp. 591–613, 1975.

[6] C. W. Monroe and J. Newman, "Onsager reciprocal relations for Stefan-Maxwell diffusion," *Ind. Eng. Chem. Res.*, vol. 45, no. 5, pp. 5361–5367, 2006.

[7] A. Parthasarathy, S. Srivinivasan, A. J. Appleby, and C. R. Martin, "Temperature dependence of the electrode kinetics of oxygen reduction at the platinum/Nafion interface—A microelectrode investigation," *J. Electrochem. Soc.*, vol. 139, no. 9, pp. 2530–2537, 1992.

[8] T. E. Springer, T. A. Zawodzinski, and S. Gottesfeld, "Polymer electrolyte fuel cell model," *J. Electrochem. Soc.*, vol. 138, no. 8, pp. 2334–2342, 1991.

[9] M. Le Ny *et al.*, "Current distribution identification in fuel cell stacks from external magnetic field measurements," in *Proc. Biennial IEEE Conf. Electromagn. Field Comput. (EFC)*, vol. 49. Ōita, Japan, 2012, pp. 1925–1928.

Authorized licensed use limited to: TONGJI UNIVERSITY. Downloaded on March 26,2024 at 08:56:07 UTC from IEEE Xplore. Restrictions apply.